Color-Coded Fluorescent Protein Imaging of Angiogenesis: The AngioMouse® Models

Yasuyuki Amoh[1,*], Kensei Katsuoka[1] and Robert M. Hoffman[2,3]

[1]*Department of Dermatology, Kitasato University School of Medicine, Sagamihara, Kanagawa, Japan;* [2]*AntiCancer, Inc., 7917 Ostrow Street, San Diego, California 92111-3604 and* [3]*Department of Surgery, University of California, San Diego, 200 West Arbor Dr., San Diego, CA 92103-8220, USA*

Abstract: We have utilized multicolored fluorescent proteins to develop three imaging models of tumor angiogenesis. In one model, the nonluminous induced capillaries are clearly visible by contrast against the very bright tumor green fluorescent protein (GFP) fluorescence examined either intravitally or by whole-body imaging in real time. Intravital images of an orthotopic model of human pancreatic tumors expressing GFP visualized angiogenic capillaries at both primary and metastatic sites. Whole-body optical imaging showed that blood vessel density increased linearly over a 20-week period in an orthotopic model of human breast cancer expressing GFP. Opening a reversible skin-flap in the light path markedly reduces signal attenuation, increasing detection sensitivity many-fold and enables vessels to be externally visualized in GFP-expressing tumors growing on internal organs. In another model, dual-color fluorescence imaging was effected by using red fluorescent protein (RFP)-expressing tumors growing in GFP-expressing transgenic mice that express GFP in all cells. This dual-color model visualizes with great clarity the details of the tumor-stroma interaction, especially tumor-induced angiogenesis. The GFP-expressing tumor vasculature, both nascent and mature, are readily distinguished interacting with the RFP-expressing tumor cells. The third model involves a transgenic mouse in which the regulatory elements of the stem cell marker nestin drive GFP (ND-GFP). The ND-GFP mouse expresses GFP in nascent blood vessels. RFP-expressing tumors transplanted to nestin-GFP mice enable specific visualization of nascent vessels. The ND-GFP mouse was utilized to develop a rapid *in vivo/ex vivo* fluorescent angiogenesis assay by implanting Gelfoam which was vascularized by fluorescent nascent blood vessels. This process could be markedly stimulated or inhibited by specific compounds. We also observed, using ND-GFP mice, that the hair follicle is angiogenic and that the hair-follicle vascular network is a prime target for chemotherapy drugs which cause hair loss (chemotherapy-induced alopecia). These fluorescent models, generally termed AngioMouse®, can quantitatively determine efficacy of antiangiogenesis compounds.

Key Words: Green fluorescent protein, red fluorescent protein, nude mouse, human tumors, imaging, nascent blood vessels.

INTRODUCTION

Previous Models Used to Determine Angiogenesis

The discovery and evaluation of antiangiogenic substances initially relied on methods such as the chorioallantoic membrane assay [1, 2], the monkey iris neovascularization model [3], the disk angiogenesis assay [4], and various models that use the cornea to assess blood vessel growth [5-10]. Although they are important for understanding the mechanisms of blood vessel induction, these models do not represent tumor angiogenesis and are poorly suited to drug discovery.

Subcutaneous tumor xenograft mouse models have been developed to study tumor angiogenesis, but these require cumbersome pathological examination procedures such as histology and immunohistochemistry. Measurements require animal sacrifice and therefore preclude ongoing angiogenesis studies in individual, live, tumor-bearing animals. Moreover, subcutaneous tumor xenografts are not representative models of human disease.

*Address correspondence to this author at the Department of Dermatology, Kitasato University School of Medicine, Sagamihara, Kanagawa, Japan; E-mail: amo@med.kitasato-u.ac.jp

Tumors transplanted in the cornea of the rodents [11-13] and rodent skin-fold window chambers have also been used for angiogenesis studies [14-20]. The cornea and skin-fold chamber models provide a means for studying tumor angiogenesis in living animals. However, quantification requires specialized procedures, and the sites do not represent natural environments for tumor growth. The cornea and skin-fold window chamber tumor models do not allow metastasis and angiogenesis to occur, which may involve mechanisms of angiogenesis [21] that are qualitatively different from those occurring in ectopic models.

We describe here clinically-relevant imageable mouse models to visualize and quantify angiogenesis and efficacy of inhibitors.

FLUORESCENT ANGIOGENESIS MODELS

Fluorescent Proteins to Image Angiogenesis

For *in vivo* imaging, a strong signal, and high resolution are necessary. The *GFP* gene, cloned from the bioluminescent jellyfish *Aequorea victoria* [22], was chosen to satisfy these conditions because it has great potential for use as a cellular marker [23, 24]. GFP cDNA encodes a 283-amino acid monomeric polypeptide with *M*r 27,000 [25, 26] that

1381-6128/08 $55.00+.00

requires no other *A. victoria* proteins, substrates, or cofactors to fluoresce [27]. Gain-of-function bright mutants expressing the *GFP* gene have been generated by various techniques [28-30] and have been humanized for high expression and signal [31]. Red fluorescent proteins (RFP) from the *Discosoma* coral have similar features as well as the advantage of longer-wavelength emission [32-34]. Our laboratory has pioneered the use of GFP for *in vivo* imaging [35] including non-invasive whole-body imaging [36, 37].

Fluorescent proteins have been shown by our laboratory to be very useful for imaging angiogenesis. We have developed three unique mouse models to image tumor angiogenesis with fluorescent proteins, which are described in this review.

Orthotopic Tumor Models Expressing Fluorescent Proteins to Visualize Tumor Angiogenesis

For realistic and real-time tumor angiogenesis models, we have developed surgical orthotopic implantation (SOI) metastatic models of human cancer [38]. These models place tumors in natural microenvironments and replicate clinical tumor behavior more closely than do ectopic implantation models [38]. The orthotopically-growing tumors, in contrast to most other models, give rise to spontaneous metastases that resemble, both in target tissues and in frequency of occurrence, the clinical behavior of the original human tumor [38]. The tumors implanted in the orthotopic model have been transduced and selected to strongly express green fluorescent protein (GFP) *in vivo* [37]. Orthotopically-implanted GFP-labeled tumors enable the visualization of the role of angiogenesis in metastasis. As Li *et al.* [18] point out, angiogenesis initiation in metastatic tumors may be very different from that of primary tumors and require different interventions. Moreover, the extreme detection sensitivity afforded by the strong GFP fluorescence allows imaging of very early events in blood vessel induction.

GFP expression in primary tumors and in their metastases in the mouse models can be detected by an intense fluorescence seen by intravital or by whole-body imaging. The nonluminous angiogenic blood vessels appear as sharply defined dark networks against this bright background. The high image resolution permits quantitative measurements of total vessel length. These genetically fluorescent tumor models thereby allow quantitative optical imaging of angiogenesis *in vivo*. Tumor growth, vascularization, and metastasis can now be followed in real time [39].

Intravital Images of Angiogenesis of Orthotopic Pancreas Cancer

The clarity of angiogenic blood vessel imaging was illustrated by intravital examination of the orthotopic growth of a Bx-PC-3-GFP pancreatic tumor. The nonluminous blood vessels were clearly visible against the GFP fluorescence of the primary tumor. Angiogenesis associated with metastatic growths was readily imaged by intravital examination [39].

Because angiogenesis could be measured without animal sacrifice, it was possible to determine a time course for individual animals. Sequential intravital images of angiogenesis for the PC-3 human prostate tumor expressing GFP and growing orthotopically in a single nude mouse were acquired. The tumor-associated blood vessels were clearly visible by day-7 and continued to increase at least until day-20 [39].

Whole-Body Imaging of Angiogenesis in Orthotopic Breast Cancer

We have demonstrated whole-body images and quantitation of the time course of angiogenesis of the MDA-MB-435-GFP human breast cancer growing orthotopically in the mammary fat pad in a nude mouse. The development of the tumor and its angiogenesis could be imaged in a completely noninvasive manner [39]. The mouse mammary fat pad is the orthotopic environment for the implanted MDA-MB-435-GFP breast cancer and allows noninvasive, whole-body imaging of tumor angiogenesis. The quantitative angiogenesis data show that microvessel density increased over 20 weeks. Thus, tumors in their natural microenvironment, growing orthotopically in sites such as the fatpad, can be whole-body imaged for quantitative angiogenesis studies [39].

Skin Flaps Enable Ultra-High Resolution External Imaging of Tumor Angiogenesis

Opening a reversible skin-flap in the light path markedly reduced signal attenuation, increasing detection sensitivity many-fold. The observable depth of tissue is thereby greatly increased [40]. The brilliance of the tumor GFP fluorescence, facilitated by the reduced absorption through the skin-flap window, allowed imaging of the induced microvessels by their contrast against a bright background. The orthotopically growing BxPC-3-GFP human pancreatic tumor was externally visualized under fluorescence microscopy to be surrounded by its microvessels visible by their dark contrast [40].

Dual-Color Tumor-Host Models to Differentially Visualize the Tumor and Blood Vessels

Okabe *et al.* [41] produced transgenic mice with GFP under the control of a chicken bet-actin promoter and cytomegalovirus enhancer. All of the tissues from these transgenic mice, with the exception of erythrocytes and hair, fluoresce green.

Tumor cells to be transplanted in the GFP mouse were made visible by transforming them with the red fluorescent protein (RFP) [42]. In order to gain further insight into tumor-host interaction in the living state, including tumor angiogenesis, we have visualized RFP-expressing tumors transplanted in the GFP-expressing transgenic mice under dual-color fluorescence microscopy. The dual-color fluorescence made it possible to visualize the tumor growth in the host by whole-body imaging as well as to visibly distinguish interacting tumor and host cells in fresh tissue. The dual-color approach affords a powerful means of both visualizing and distinguishing the components of the host-tumor interaction [42].

Dual-color images of early events in tumor angiogenesis induced by a B16F10 mouse melanoma in the transgenic GFP-expressing mouse were acquired in fresh tissue preparations. Host-derived GFP-expressing fibroblast cells and

endothelial cells from nascent blood vessels were visualized clearly against the red fluorescent background of the RFP-expressing mouse melanoma. Host-derived GFP-expressing mature blood vessels within the RFP-expressing mouse melanoma also became visible. The images were acquired 3 weeks after subcutaneous injection of B16F10-RFP melanoma cells in the GFP mouse [42].

Imaging of Nascent Angiogenesis Using Nestin-Driven GFP Transgenic Mice

We initially reported that in mice in which the gene for the stem cell marker nestin-driven GFP (ND-GFP), that ND-GFP also labels developing skin blood vessels that appear to originate from hair follicles and form a follicle-linking network. This was seen most clearly by transplanting NDGFP-labeled vibrissa (whisker) hair follicles to unlabeled nude mice. New vessels grew from the transplanted follicle, and these vessels increased when the local recipient skin was wounded. The ND-GFP-expressing structures are blood vessels, because they display the characteristic endothelial-cell-specific markers CD31 and von Willebrand factor. This model displays very early events in skin angiogenesis and can serve for rapid antiangiogenesis drug screening [43].

We visualized tumor angiogenesis by dual-color fluorescence imaging in ND-GFP transgenic mice after transplantation of the murine melanoma cell line B16F10 expressing RFP. ND-GFP was highly expressed in proliferating endothelial cells and nascent blood vessels in the growing tumor (Fig. **1**). Results of immunohistochemical staining showed that the blood vessel-specific antigen CD31 was expressed in ND-GFP-expressing nascent blood vessels. ND-GFP expression was diminished in the vessels with increased blood flow. Progressive angiogenesis during tumor growth was readily visualized during tumor growth by GFP expression. Doxorubicin inhibited the nascent tumor angiogenesis as well as tumor growth in the ND-GFP mice transplanted with B16F10-RFP [44].

The nestin ND-GFP gene was crossed into nude mice on the C57/B6 background to obtain ND-GFP nude mice. ND-GFP was expressed in the brain, spinal cord, pancreas, stomach, esophagus, heart, lung, blood vessels of glomeruli, blood vessels of skeletal muscle, testis, hair follicles, and blood vessel network in the skin of ND-GFP nude mice. Human lung cancer, pancreatic cancer, breast and colon cancer cell lines as well as a murine melanoma cell line expressing RFP were implanted orthotopically, and a RFP-expressing human fibrosarcoma was implanted s.c. in the ND-GFP nude mice (Fig. **2**). These tumors grew extensively in the ND-GFP mice. ND-GFP was highly expressed in proliferating endothelial cells and nascent blood vessels in the growing tumors, visualized by dual-color fluorescence imaging (Fig. **3**). The ND-GFP transgenic nude mouse model enables the visualization of nascent angiogenesis in human and mouse tumor progression [45].

Dual-color fluorescence imaging visualized tumor angiogenesis in the ND-GFP transgenic nude mice after orthotopic transplantation of the MIA PaCa-2 human pancreatic cancer line expressing RFP. Mice were treated with gemcitabine at 150 mg/kg/dose on days 3, 6, 10, and 13 after tumor implantation. At day 14, mice were sacrificed and mean nascent blood vessel density and tumor volume were calculated and compared to control mice. The density of nascent blood vessels in the tumor was readily quantitated. Gemcitabine significantly decreased the mean nascent blood vessel density in the tumor as well as decreased tumor volume. The dual-color model of the ND-GFP nude mouse orthotopically implanted

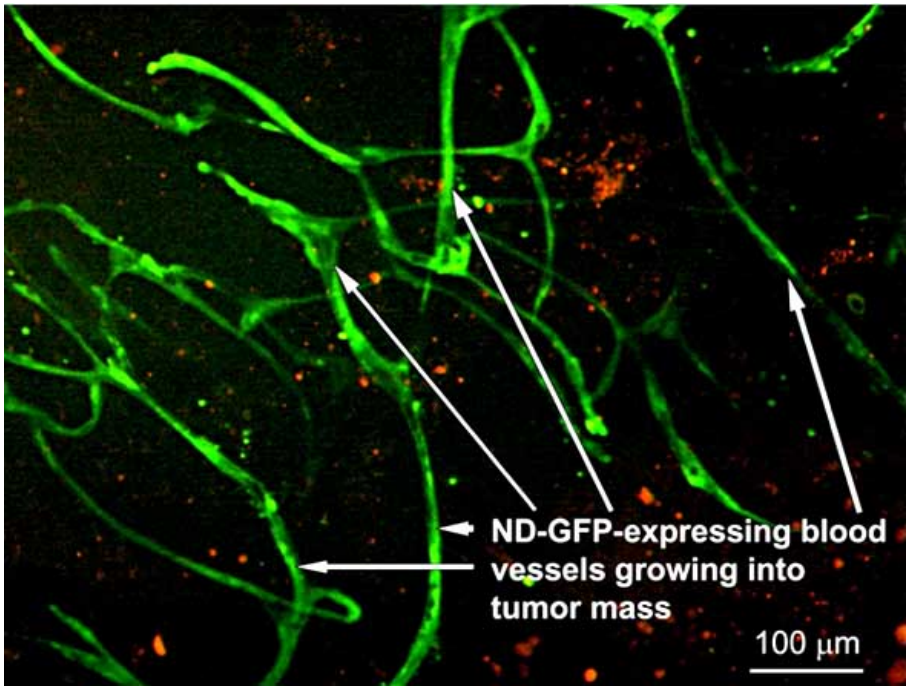

Fig. (1). On day 14 after implantation of RFP-expressing mouse melanoma cells subcutaneously, ND-GFP-expressing blood vessels (white arrows) could be seen in the growing tumor. After implantation of RFP-expressing mouse melanoma cells subcutaneously, nascent ND-GFP blood vessels (white arrows) were forming a network in the growing tumor. At day 14 after tumor-cell implantation, the ND-GFP blood vessels were forming networks in the growing RFP tumors. Bar, 100 μm [44].

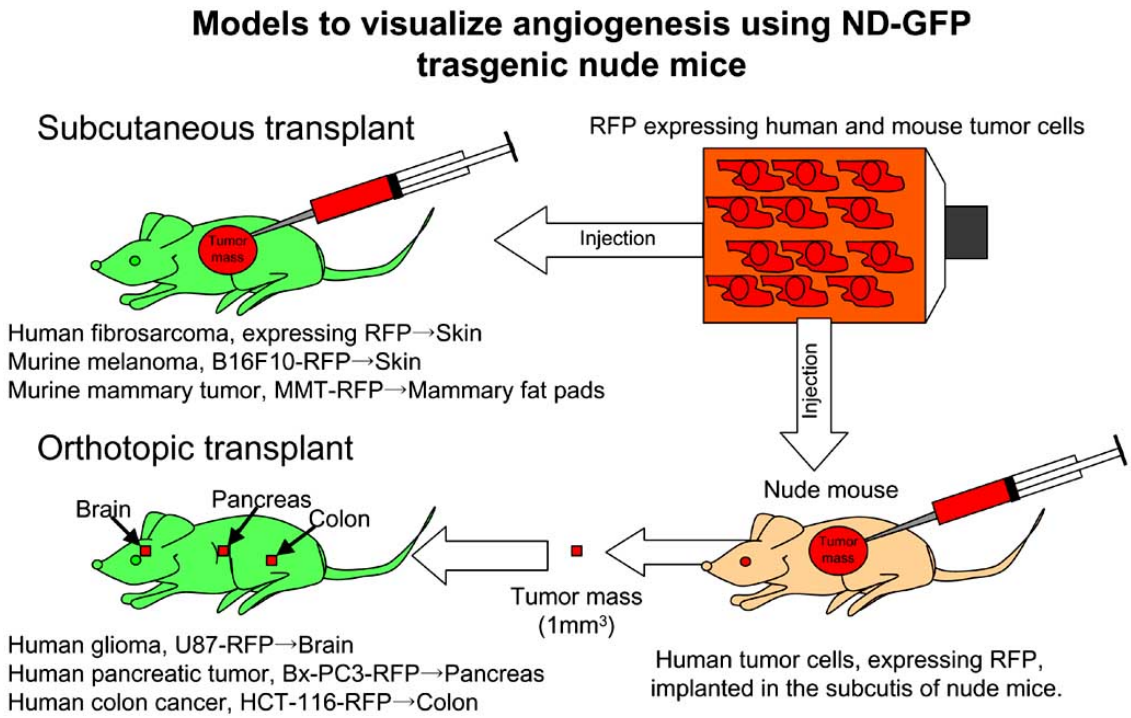

Fig. (2). Color-coded fluorescent imaging of angiogenesis using ND-GFP trasgenic nude mice. Human lung cancer, pancreatic cancer, and colon cancer cell lines expressing red fluorescent protein were implanted orthotopically, and human fibrosarcoma, murine melanoma and breast cancer tumor cell lines expressing red fluorescent protein were implanted subcutaneously in the ND-GFP transgenic nude mice [45].

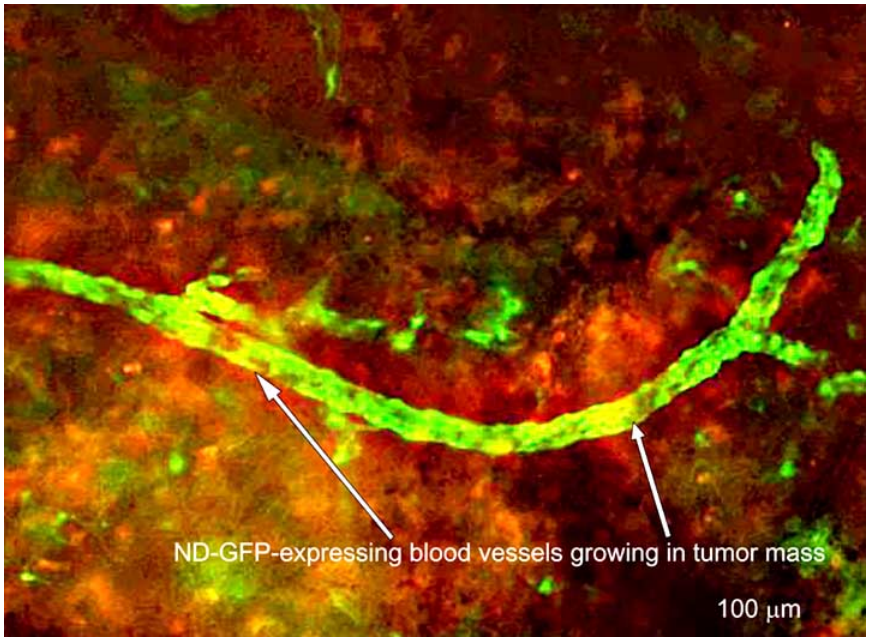

Fig. (3). Fluorescence imaging of tumor angiogenesis in transgenic ND-GFP nude mice. Human HT1080 fibrosarcoma on day 14 after s.c. injection. Dual-color tumor cells expressing GFP in the nucleus and RFP in the cytoplasm are polarized towards ND-GFP-expressing blood vessels (white arrows) growing in the tumor mass. Bar, 100 μm [45].

with RFP-expressing pancreatic tumor cells enabled the simultaneous visualization and quantitation of tumor angiogenesis and tumor volume. These results demonstrated for the first time that gemcitabine is an inhibitor of angiogenesis as well as tumor growth in pancreatic cancer. The results have important implications for the clinical application of gemcitabine in this disease [46].

Nascent angiogenesis was imaged in pancreatic cancer liver metastasis in the ND-GFP transgenic nude mice, formed after intra-splenic injection of xPA-1 human pancreatic cancer cells expressing RFP, using dual-color fluorescence. ND-GFP was highly expressed in proliferating endothelial cells and nascent blood vessels in the growing liver metastasis. The density of nascent blood vessels in the tumor

was readily quantitated. Gemcitabine significantly decreased the mean nascent blood vessel density in the pancreatic liver metastases [47].

Angiogenesis in experimental lung and liver metastases was imaged in the ND-GFP transgenic mice. The murine melanoma cell line, B16F10 expressing RFP, was injected i.v. in ND-GFP mice. ND-GFP was highly expressed in proliferating nascent blood vessels in the tumors that developed in the lung after tail vein injection, and in the tumors that developed in the liver after portal vein injection of RFP-expressing melanoma cells. Liver metastasis and angiogenesis were imaged intravitally (Fig. **4**). Doxorubicin significantly decreased metastatic angiogenesis (Fig. **5**) [48].

The antiangiogenic efficacy of CPT-11 was evaluated in ND-GFP nude mice using dual-color fluorescence imaging. We orthotopically implanted ND-GFP nude mice with the human cancer cell line HCT-116 expressing RFP. The mice were treated with CPT-11 at 40 mg/kg on days 7, 10, 14. Tumor angiogenesis was imaged and visualized by dual-color fluorescence imaging on day 17, three days after the last CPT-11 treatment. Tumor volume and the mean nascent blood vessel density were determined and compared to the control mice. The nascent blood vessels were highly fluorescent and their density was determined. ND-GFP nude mice that were administered CPT-11 showed significant reduction in the mean nascent blood vessel density and tumor volume. The results showed that CPT-11 is an effective inhibitor of angiogenesis and provided strong implications for wider clinical application of CPT-11 for colon cancer [49].

Angiogenesis of the HT-1080 human fibrosarcoma cell line, expressing RFP, was imaged in the ND-GFP mice. Tumor cells were injected into either the muscle or the bone. Nestin was highly expressed in proliferating endothelial cells and nascent blood vessels in the growing tumors, including the surrounding tissues. CD31 colocalized in ND-GFP-expressing nascent blood vessels. The density of nascent blood vessels in the tumor was readily quantitated. The mice were given daily i.p. injections of 5 mg/kg doxorubicin after implantation of tumor cells. Doxorubicin significantly decreased the mean nascent blood vessel density in the tumors as well as decreased tumor volume. These data suggest targeting angiogenesis of sarcomas as a promising clinical approach [50].

Imageable Model of Lymphangiogenesis

Cancer cells labeled with both GFP in the nucleus and RFP in the cytoplasm or with GFP only or RFP only were injected into the inguinal lymph node of nude mice. The labeled cancer cells trafficked through lymphatic vessels where they were imaged *via* a skin flap in real time at the cellular level until they entered the axillary lymph node. The bright fluorescence of the cancer cells and the real-time microscopic imaging capability of the Olympus OV100 small-animal imaging system enabled imaging of the trafficking cancer cells in the lymphatics. Using this imaging technology, we also investigated the role of pressure on tumor-cell shedding into lymphatic vessels. Pressure was generated by placing 25- and 250-g weights for 10 s on the bottom surface of a tumor-bearing footpad. Tumor cell fragments, single cells, and emboli shed from the footpad tumor were easily distinguished with the labeled cells and OV100 imaging system. Increasing pressure on the tumor increased the number of shed cells, fragments, and emboli. Pressure also deformed the shed emboli, increasing their maximum major axis. Imaging lymphatic trafficking of cancer cells can reveal critical steps of lymph node metastasis [51].

We have utilized monoclonal antibodies and fluorescent proteins, respectively, to color-code lymphatic vessels and the cancer cells inside them in a living animal. Monoclonal anti-mouse LYVE-1 antibody was conjugated to a green

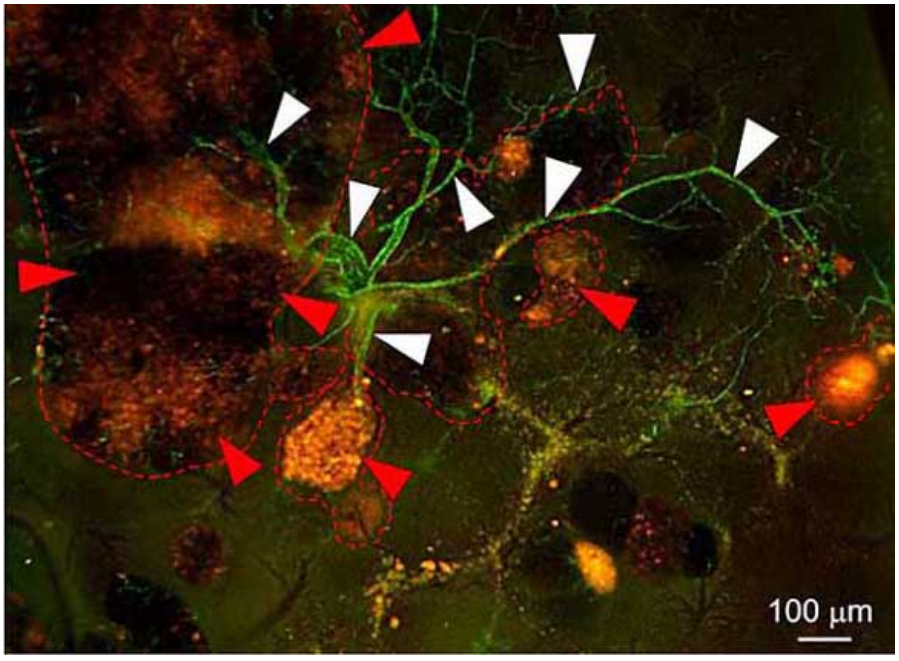

Fig. (4). On day 15 after injection of RFP-expressing mouse melanoma cells into portal vein, newly formed ND-GFP-expressing blood vessels (white arrowheads) are growing along the RFP-expressing tumor in the liver (red arrowheads) [48].

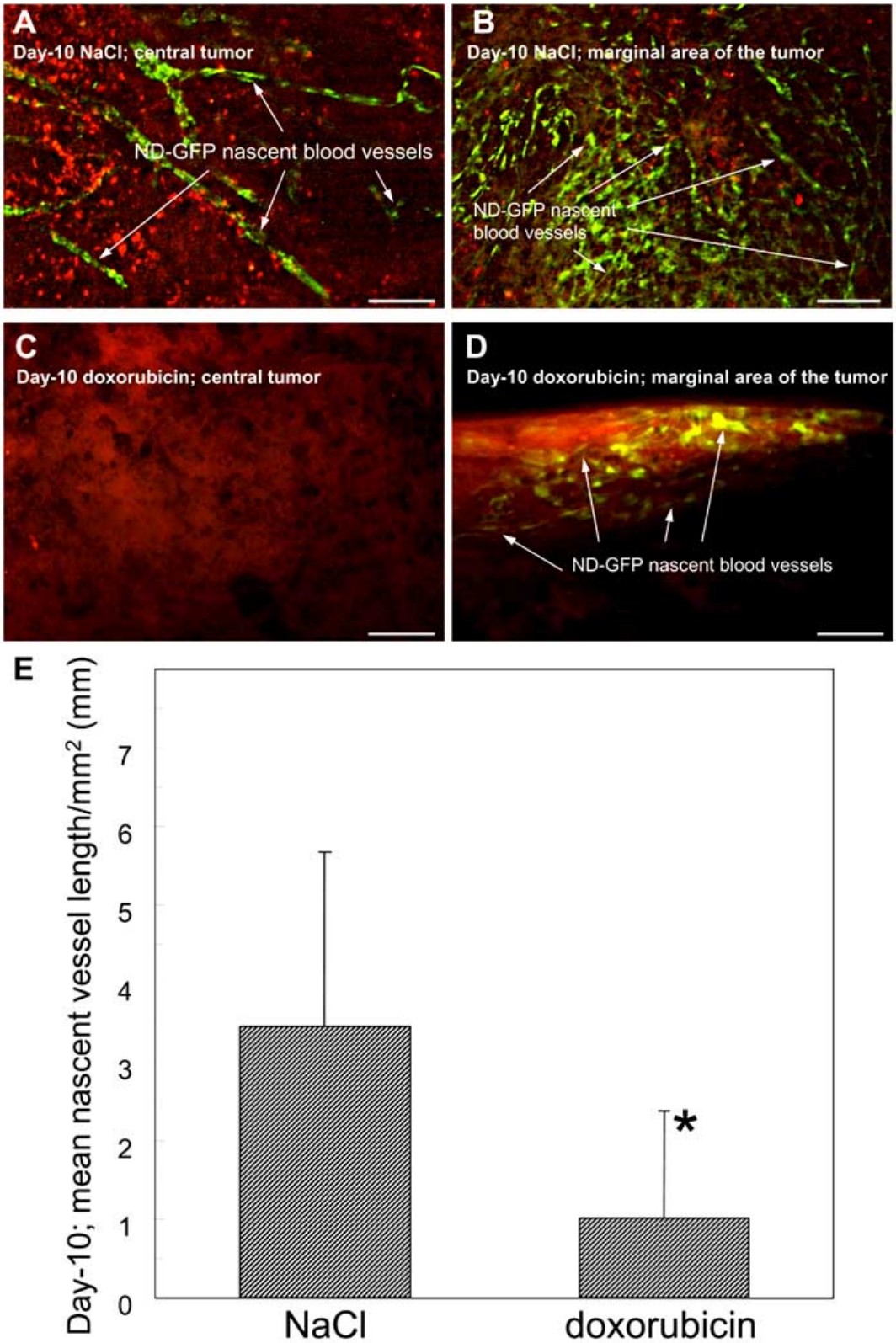

Fig. (5). Effect of doxorubicin on tumor angiogenesis. **A**, on day 10 after implantation of tumor cells, the ND-GFP nascent blood vessels (white arrows) were forming a network in the central tumor. **B**, in the marginal area of the tumor, many newly-formed nascent ND-GFP blood vessels were growing. The nascent ND-GFP blood vessels (white arrows) had many branches and were connected to each other. **C** and **D**, the mice were given daily i.p. injections of 5 μg/g of doxorubicin at days 0, 1, and 2 after implantation of tumor cells. **C**, by day 10 after implantation of tumor cells, the nascent ND-GFP blood vessels were not seen in the central area of the tumor. **D**, in the marginal area of the tumor, ND-GFP blood vessels (white arrows) were growing slightly. **E**, number of nascent blood vessels per tumor volume was less than NaCl solution-injected mice ($P < 0.05$). Bars, 100 μm [44].

fluorophore and delivered to the lymphatic system of a nude mouse, allowing imaging of mouse lymphatics. Tumor cells expressing RFP were then imaged traveling within the labeled lymphatics in real time. AlexaFluor-labeled monoclonal anti-mouse LYVE-1 created a durable signal with clear delineation of lymphatic architecture. The duration of fluorescent signal after conjugated LYVE-1 delivery was far superior to that of FITC Dextran or control fluorophore-conjugated IgG. Tumor cells engineered to express RFP delivered to the inguinal region enabled real-time trafficking of tumor cell movement within the green fluorescent-labeled lymphatic vessels. This technology offers a powerful tool for the *in vivo* study of real-time trafficking of tumor cells within lymphatic vessels, the deposition of the tumor cells in lymph nodes, as well as for screening of potential anti-tumor-lymphatic therapies [52].

Nestin-Expressing Hair-Follicle Stem Cells are Angiogenic

We have shown that nestin is expressed in hair follicle stem cells in ND-GFP mice and is expressed in a dermal microvasculature network (Fig. **6**). Furthermore, ND-GFP was visualized by fluorescence in proliferating endothelial cells and nascent vessels. ND-GFP also labels developing skin blood vessels that appear to originate from hair follicles and form a follicle-linking network. This is seen most clearly by transplanting NDGFP-labeled vibrissa (whisker) hair follicles to unlabeled nude mice. New vessels grow from the transplanted follicle, and these vessels increase when the local recipient skin is wounded. The ND-GFP-expressing structures are blood vessels, because they display the characteristic endothelial-cell-specific markers CD31 and von Willebrand factor. This model displays very early events in skin angiogenesis and can serve for rapid antiangiogenesis drug screening [43].

Chemotherapy Targets the Hair-Follicle Vascular Network

Chemotherapy can induce anagen hair follicles to develop abnormalities that are termed hair-follicle dystrophy [53-55]. The hair-follicle vascular network has an important role in hair-follicle cycling.

Doxorubicin causes disruption of the hair-follicle-associated blood vessel network resulting in a greatly reduced density of these blood vessels. Dystrophic hair follicles were also observed with abnormal melanogenesis in the mice treated with doxorubicin. Visualization of the effects of doxorubicin on hair-follicle angiogenesis was made possible by the use of ND-GFP mice. The hair-follicle stem cells did not appear to be affected by doxorubicin, which may explain why hair regrows after chemotherapy. These results suggest that inhibition of hair-follicle-associated angiogenesis by doxorubicin may be an important factor in hair-follicle dystrophy associated with chemotherapy-induced alopecia. The

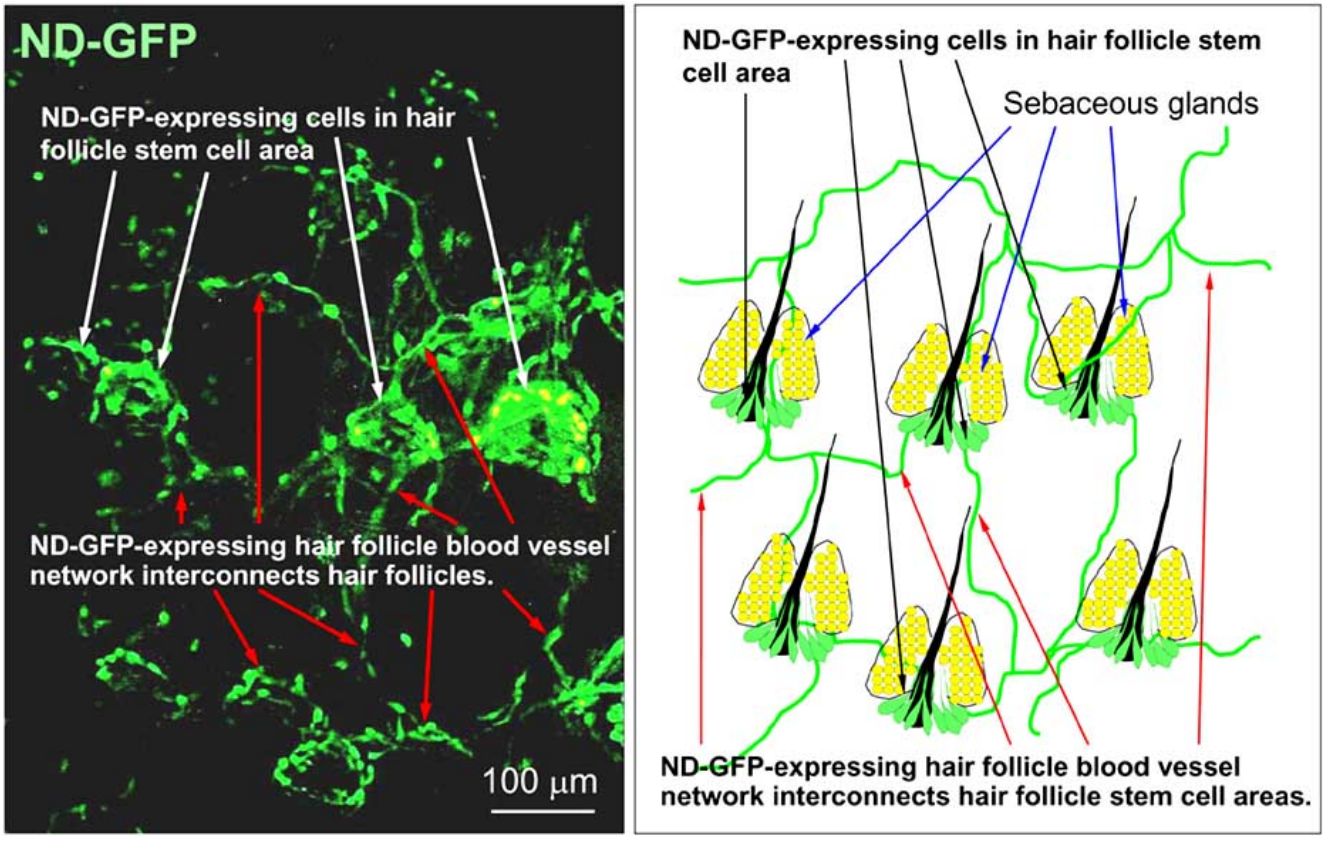

Fig. (6). ND-GFP-expressing hair follicles are interconnected by an ND-GFP-labeled dermal vascular network visualized in ND-GFP transgenic mice. View is from the dermis side imaged with a confocal fluorescent microscope [43].

ND-GFP mouse model is thus useful for the study of the role of angiogenesis in the hair-follicle cycle and the effect of drugs on processes associated with chemotherapy-induced alopecia [56].

Rapid *In Vivo/Ex Vivo* Nascent Angiogenesis Assay

We developed a very convenient imageable *in vivo* angiogenesis assay after transplantation of Gelfoam® (Pharmacia & Upjohn Company, Kalamazoo, MI, USA) in the ND-GFP mice [57]. Gelfoam is rapidly vascularized with GFP-expressing vessels in the presence of an angiogenesis stimulator. Anti-angiogenesis agents inhibit this process. Thus, this rapid and simple new *in vivo* assay can rapidly identify angiogenesis stimulators and inhibitors. Gelfoam was treated with and without β fibroblast growth factor. The treated Gelfoam was then transplanted into the subcutis on both flanks of the ND-GFP transgenic mice. The mice were given daily intraperitoneal (ip) injections of doxorubicin or NaCl solution at day 0, 1, and 2 after transplantation of Gelfoam. Skin flaps were made at day 7 after transplantation of Gelfoam under anesthesia. Angiogenesis was quantified by measuring the length of ND-GFP-expressing nascent blood vessels in the Gelfoam in the skin flap by *in vivo* fluorescence microscopy imaging (Fig. **7**). The vessels on the surface were counted under fluorescence microscopy. Each experimental group consisted of five mice. Co-localization of ND-GFP fluorescence and CD31 in frozen sections of the vascularized Gelfoam was observed. Gelfoam implanted in the ND-GFP mice was rapidly vascularized with ND-GFP-expressing blood vessels. Angiogenesis was quantified in the Gelfoam by measuring the total length of ND-GFP-expressing nascent blood vessels by fluorescence imaging. At day 7 after transplantation, the NDGFP-expressing nascent blood vessels were observed forming a network on the surface of the bFGF-treated Gelfoam in the skin flap (Fig. **7**). Implanted Gelfoam that was not treated with bFGF was not vascularized. The ND-GFP vessels in the Gelfoam stained positively for CD31, demonstrating the presence of endothelial cells. Day 7 was chosen as an arbitrary time point to measure the GFP vessels in the implanted Gelfoam. The Gelfoam can be analyzed at any time point, and an optimal time for measurement would depend on the angiogenesis drug being tested. ND-GFP mice that received ip injections of doxorubicin (5 μg/g) at day 0, 1, and 2 after transplantation of Gelfoam, with or without bFGF, had fewer ND-GFP-expressing nascent blood vessels than NaCl-treated mice [57]. Future experiments will address the destruction of preformed vessels in Gelfoam by vascular disrupting agent (VDA) [58].

CONCLUSIONS

This review demonstrates the power of fluorescent proteins to visualize angiogenesis in mouse models. The ability to color code blood vessels, including nascent vessels, and their associated tumor cells, adds exquisite resolution to fluorescence imaging technology. Fluorescence imaging technology can additionally be applied to visualize lymphatic vessels. The technology is well suited to readily evaluate inhibitors and stimulators of angiogenesis in the living

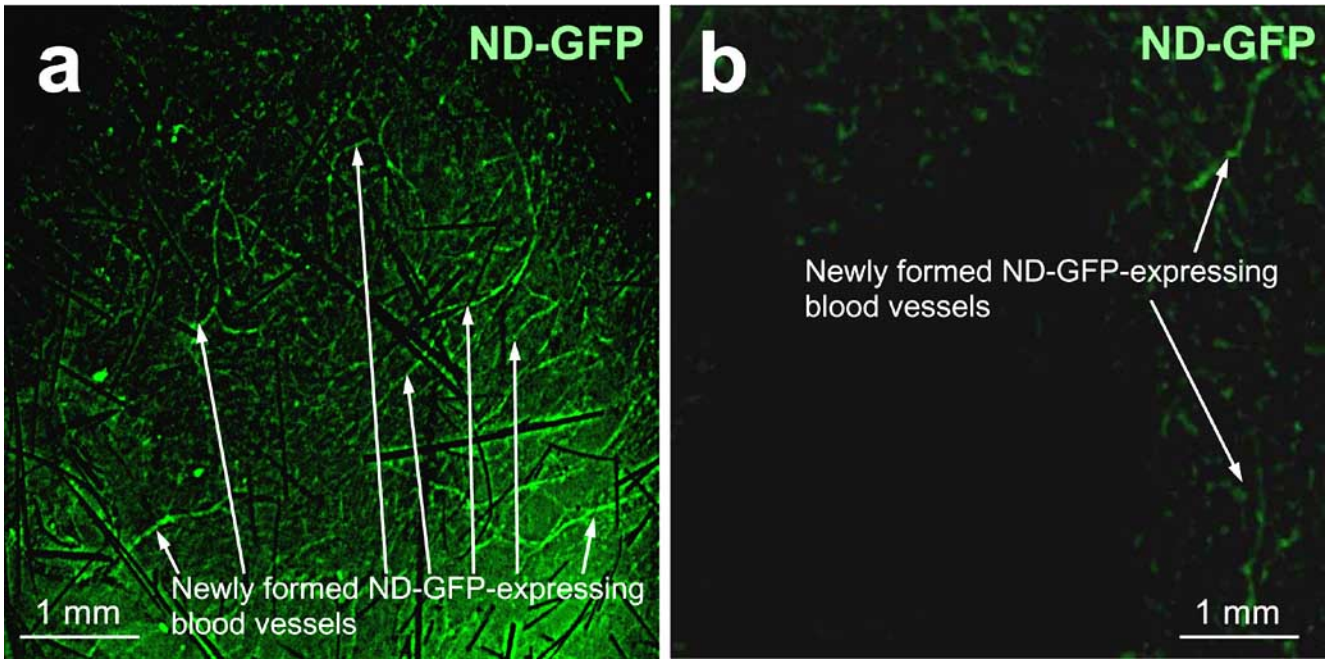

Fig. (7). Angiogenesis of implanted Gelfoam with GFP-expressing vessels. NDGFP mice were given daily intraperitoneal (ip) injections of 0.9% NaCl solution at day 0, 1, and 2 after transplantation of Gelfoam with or without β fibroblast growth factor (bFGF). (**a**) At day 7 after transplantation of Gelfoam with bFGF, the ND-GFP-expressing nascent blood vessels formed a network on the surface of Gelfoam in the skin flap. The ND-GFP-expressing nascent blood vessels had many branches that were connected to each other. (**b**) The Gelfoam-transplanted ND-GFP mice were treated with 5 μg/g doxorubicin (DOX) at day 0, 1, and 2 after transplantation. Doxorubicin significantly decreased the blood-vessel density in the presence of bFGF at day 7. Scale bar, 500 μm [58].

mouse. We can expect important new anti-angiogenesis drugs to be discovered in the future with the technology described in this review.

ACKNOWLEDGEMENT

These studies were funded in part by National Cancer Institute grant numbers CA099258, CA103563, and CA101600.

ABBREVIATIONS

bFGF = Basic Fibroblast Growth Factor

GFP = Green Fluorescent Protein

I.P. = Intraperitoneal

ND-GFP = Nestin-regulatory-element-driven Green Fluorescent Protein

RFP = Red Fluorescent Protein

SOI = Surgical Orthotopic Implantation

VEGF = Vascular Endothelial Growth Factor

REFERENCES

[1] Auerbach R, Kubai L, Knighton D, Folkman J. A simple procedure for the long-term cultivation of chicken embryos. Dev Biol 1974; 41: 391-4.

[2] Crum R, Szabo S, Folkman J. A new class of steroids inhibits angiogenesis in the presence of heparin or a heparin fragment. Science 1985; 230: 1375-8.

[3] Miller JW, Stinson WG, Folkman J. Regression of experimental iris neovascularization with systemic alpha-interferon. Ophthalmology 1993; 100: 9-14.

[4] Passaniti A, Taylor RM, Pili R, Guo Y, Long PV, Haney JA, *et al.* A simple, quantitative method for assessing angiogenesis and antiangiogenic agents using reconstituted basement membrane, heparin, and fibroblast growth factor. Lab Invest 1992; 67: 519-28.

[5] Alessandri G, Raju K, Gullino PM. Mobilization of capillary endothelium *in vitro* induced by effectors of angiogenesis *in vivo*. Cancer Res 1983; 43: 1790-7.

[6] Deutsch TA, Hughes WF. Suppressive effects of indomethacin on thermally induced neovascularization of rabbit corneas. Am J Ophthalmol 1979; 87: 536-40.

[7] Korey M, Peyman GA, Berkowitz R. The effect of hypertonic ointments on corneal alkali burns. Ann Ophthalmol 1977; 9: 1383-7.

[8] Mahoney J M, Waterbury LD. Drug effects on the neovascularization response to silver nitrate cauterization of the rat cornea. Curr Eye Res 1985; 4: 531-5.

[9] Li WW, Grayson G, Folkman J, D'Amore PA. Sustained-release endotoxin. A model for inducing corneal neovascularization. Invest Ophthalmol Vis Sci 1991; 32: 2906-11.

[10] Epstein RJ, Hendricks RL, Stulting RD. Interleukin-2 induces corneal neovascularization in A/J mice. Cornea 1990; 9: 318-23.

[11] Gimbrone MA Jr, Cotran RS, Leapman SB, Folkman J. Tumor growth and neovascularization: an experimental model using the rabbit cornea. J Natl Cancer Inst 1974; 52: 413-27.

[12] Fournier GA, Lutty GA, Watt S, Fenselau A, Patz A. A corneal micropocket assay for angiogenesis in the rat eye. Invest Ophthalmol Vis Sci 1981; 21: 351-4.

[13] Muthukkaruppan V, Auerbach R. Angiogenesis in the mouse cornea. Science 1979; 205: 1416-8.

[14] Papenfuss HD, GrossJF, Intaglietta M, Treese FA. A transparent access chamber for the rat dorsal skin fold. Microvasc Res 1979; 18: 311-8.

[15] Shan S, Robson ND, Cai Y, Qiao T, Li CY, Kontos CD, *et al.* Responses of vascular endothelial cells to angiogenic signaling are important for tumor cell survival. FASEB J 2004; 18: 326-8.

[16] Dewhirst M, Gross J, Sim D, Arnold P, Boyer D. The effect of rate of heating or cooling prior to heating on tumor and normal tissue microcirculatory blood flow. Biorheology 1984; 21: 539-58.

[17] Fukumura D, Xavier R, Sugiura T, Chen Y, Park EC, Lu N, *et al.* Tumor induction of VEGF promoter activity in stromal cells. Cell 1998; 94: 715-25.

[18] Li CY, Shan S, Huang Q, Braun R D, Lanzen J, Hu K, *et al.* Initial stages of tumor cell-induced angiogenesis: evaluation *via* skin window chambers in rodent models. J Natl Cancer Inst 2000; 92: 143-7.

[19] Al-Mehdi AB, Tozawa K, Fisher AB, Shientag L, Lee A, Muschel RJ. Intravascular origin of metastasis from the proliferation of endothelium-attached tumor cells: a new model for metastasis. Nat Med 2000; 6: 100-2.

[20] Huang Q, Shan S, Braun RD, Lanzen J, Anyrhambatla G, Kong G, *et al.* Noninvasive visualization of tumors in rodent dorsal skin window chambers. Nat Biotechnol 1999; 17: 1033-5.

[21] Cowen,SE, Bibby MC, Double JA. Characterisation of the vasculature within a murine adenocarcinoma growing in different sites to evaluate the potential of vascular therapies. Acta Oncol 1995; 34: 357-60.

[22] Prasher DC, Eckenrode VK, Ward WW, Prendergast FG, Cormier MJ. Primary structure of the Aequorea victoria green-fluorescent protein. Gene 1992; 111: 229-33.

[23] Chalfie M, Tu Y, Euskirchen G, Ward WW, Prasher DC. Green fluorescent protein as a marker for gene expression. Science 1994; 263: 802-5.

[24] Cheng L, Fu J, Tsukamoto A, Hawley RG. Use of green fluorescent protein variants to monitor gene transfer and expression in mammalian cells. Nat Biotechnol 1996; 14: 606-9.

[25] Cody CW, Prasher DC, Westler WM, Prendergast FG, Ward WW. Chemical structure of the hexapeptide chromophore of the Aequorea green fluorescent protein. Biochemistry 1993; 32: 1212-8.

[26] Yang F, Moss LG, Phillips GN Jr. The molecular structure of green fluorescent protein. Nat Biotechnol 1996; 14: 1246-51.

[27] Morin J, Hastings J. Energy transfer in a bioluminescent system. J Cell Physiol 1971; 77: 313-8.

[28] Cormack B, Valdivia R, Falkow S. FACS-optimized mutants of the green fluorescent protein (GFP). Gene 1996; 173: 33-8.

[29] Crameri A, Whitehorn EA, Tate E, Stemmer WP. Improved green fluorescent protein by molecular evolution using DNA shuffling. Nat Biotechnol 1996; 14: 315-9.

[30] Delagrave S, Hawtin RE, Silva CM, Yang MM, Youvan DC. Red-shifted excitation mutants of the green fluorescent protein. Biotechnology 1995; 13: 151-4.

[31] Heim R, Cubitt AB, Tsien RY. Improved green fluorescence. Nature 1995; 373: 663-4.

[32] Zolotukhin S, Potter M, Hauswirth WW, Guy J, Muzyczka N. A 'humanized' green fluorescent protein cDNA adapted for high-level expression in mammalian cells. J Virol 1996; 70: 4646-54.

[33] Gross LA, Baird GS, Hoffman RC, Baldridge KK, Tsien RY. The structure of the chromophore within DsRed, a red fluorescent protein from coral. Proc Natl Acad Sci USA 2000; 97: 11990-5.

[34] Fradkov AF, Chen Y, Ding L, Barsova EV, Matz MV, Lukyanov SA. Novel fluorescent protein from Discosoma coral and its mutants possesses a unique far-red fluorescence. FEBS Lett 2000; 479: 127-30.

[35] Chishima T, Miyagi Y, Wang X, Yamaoka H, Shimada H, Moossa AR, *et al*. Cancer invasion and micrometastasis visualized in live tissue by green fluorescent protein expression. Cancer Res 1997; 57: 2042-7.

[36] Yang M, Baranov E, Jiang P, Sun FX, Li XM, Hasegawa S, *et al.* Whole-body optical imaging of green fluorescent protein-expressing tumors and metastases. Proc Natl Acad Sci USA 2000; 97: 1206-11.

[37] Hoffman RM. Green fluorescent protein imaging of tumour growth, metastasis, and angiogenesis in mouse models. Lancet Oncol 2002; 3: 546-56.

[38] Hoffman RM. Orthotopic metastatic mouse models for anticancer drug discovery and evaluation: a bridge to the clinic. Invest New Drugs 1999; 17: 343-59.

[39] Yang M, Baranov E, Li XM, Wang JW, Jiang P, Li L, *et al.* Whole-body and intravital optical imaging of angiogenesis in orthotopically implanted tumors. Proc Natl Acad Sci USA 2001; 98: 2616-21.

[40] Yang M, Baranov E, Wang JW, Jiang P, Wang X., Sun FX, *et al*. Direct external imaging of nascent cancer, tumor progression, angiogenesis, and metastasis on internal organs in the fluorescent orthotopic model. Proc Natl Acad Sci USA 2002; 99: 3824-9.

[41] Okabe M, Ikawa M, Kominami K, Nakanishi T, Nishimune Y. 'Green mice' as a source of ubiquitous green cells. FEBS Lett 1997; 407: 313-9.

[42] Yang M, Li L, Jiang P, Moossa AR, Penman S, Hoffman RM. Dual-color fluorescence imaging distinguishes tumor cells from induced host angiogenic vessels and stromal cells. Proc Natl Acad Sci USA 2003; 100: 14259-62.

[43] Amoh Y, Li L, Yang M, Moossa AR, Katsuoka K, Penman S, *et al.* Nascent blood vessels in the skin arise from nestin-expressing hair follicle cells. Proc Natl Acad Sci USA 2004; 101: 13291-5.

[44] Amoh Y, Li L, Yang M, Jiang P, Moossa AR, Katsuoka K, *et al*. Hair follicle-derived blood vessels vascularize tumors in skin and are inhibited by doxorubicin. Cancer Res 2005; 65: 2337-43.

[45] Amoh Y, Yang M, Li L, Reynoso J, Bouvet M, Moossa AR, *et al*. Nestin-linked green fluorescent protein transgenic nude mouse for imaging human tumor angiogenesis. Cancer Res 2005; 65: 5352-7.

[46] Amoh Y, Li L, Tsuji K, Moossa AR, Katsuoka K, Hoffman RM, *et al.* Dual-color imaging of nascent blood vessels vascularizing pancreatic cancer in an orthotopic model demonstrates antiangiogenesis efficacy of gemcitabine. J Surgical Research 2006; 132: 164-9.

[47] Amoh Y, Nagakura C, Maitra A, Moossa AR, Katsuoka K, Hoffman RM, *et al.* Dual-color imaging of nascent angiogenesis and its inhibition in liver metastases of pancreatic cancer. Anticancer Res 2006; 26: 3237-42.

[48] Amoh Y, Bouvet M, Li L, Tsuji K, Moossa AR, Katsuoka K, *et al*. Visualization of nascent tumor angiogenesis in lung and liver metastasis by differential dual-color fluorescence imaging in nestin-linked-GFP mice. Clin Exp Metastasis 2006; 23(7-8): 315-22.

[49] Ji Y, Hayashi K, Amoh Y, Tsuji K, Yamauchi K, Yamamoto N, *et al.* The camptothecin derivative CPT-11 inhibits angiogenesis in a dual-color imageable orthotopic metastatic nude mouse model of human colon cancer. Anticancer Res 2007; 27: 713-8.

[50] Hayashi K, Yamauchi K, Yamamoto N, Tsuchiya H, Tomita K, Amoh Y, *et al.* Dual-color imaging of angiogenesis and its inhibition in bone and soft tissue sarcoma. J Surg Res 2007; 140: 165-70.

[51] Hayashi K, Jiang P, Yamauchi K, Yamamoto N, Tsuchiya H, Tomita K, *et al*. Real-time imaging of tumor-cell shedding and trafficking in lymphatic channels. Cancer Res 2007; 67: 8223-8.

[52] McElroy M, Hayashi K, Garmy-Susini B, Kaushal S, Varner JA, Moossa AR, *et al.* Imaging with fluorescent LYVE-1 to visualize lymphatic trafficking of cancer. J Surg Res 2008; In press.

[53] Mecklenburg L, Tobin DJ, Muller-Rover S, Handjiski B, Wendt G, Peters EM, *et al.* Active hair growth (anagen) is associated with angiogenesis. J Invest Dermatol 2000; 114: 909-16.

[54] Yano K, Brown LF, Detmar M. Control of hair growth and follicle size by VEGF-mediated angiogenesis. J Clin Invest 2001; 107: 409-17.

[55] Bodo E, Tobin DJ, Kamenisch Y, Biro T, Berneburg M, *et al.* Dissecting the impact of chemotherapy on the human hair follicle: a pragmatic *in vitro* assay for studying the pathogenesis and potential management of hair follicle dystrophy. Am J Pathol 1007; 17: 1153-67.

[56] Amoh Y, Li L, Katsuoka K, Hoffman RM. Chemotherapy targets the hair-follicle vascular network but not the stem cells. J Invest Dermatol 2007; 127: 11-5

[57] Amoh Y, Li L, Katsuoka K, Bouvet M, Hoffman RM. GFP-expressing vascularization of Gelfoam® as a rapid *in vivo* assay of angiogenesis stimulators and inhibitors. Biotechniques 2007; 42: 294-8.

[58] Shaked Y, Ciarrocchi A, Franco M, Lee CR, Man S, Cheung AM, *et al.* Therapy-induced acute recruitment of circulating endothelial progenitor cells to tumors. Science 2006; 313(5794): 1785-7.